In-situ characterization of continuous dynamic recrystallization during hot torsion of an Al-Si-Mg alloy

David Canelo-Yubero[a,b]

Zsolt Kovács[c]

J.F. Thierry Simonet Fotso[a]

Domonkos Tolnai[d]

Norbert Schell[d]

Istvan Groma[c]

Cecilia Poletti[a]

[a] Graz University of Technology, Institute of Materials Science, Joining and Forming, Kopernikusgasse 24/I, 8010 Graz, Austria

[b] Nuclear Physics Institute ASCR, CZ-25068 Řež near Prague, Czech Republic

[c] Department of Materials Physics, Institute of Physics, Eötvös Loránd University, 1117, Pázmány Péter sétány 1/A., Budapest, Hungary

[d] Institute of Materials Research, Helmholtz-Zentrum Geesthacht, Max-Planck-Str. 1, 21502 Geesthacht, Germany

Abstract

An extruded Al-Si-Mg alloy was deformed by torsion at 400°C during in-situ high energy synchrotron radiation diffraction. This technique is used to prove, by analysing texture changes and the coherently scattering domain size evolution, that dynamic recovery followed by continuous dynamic recrystallization are the main restoration mechanisms. Moreover, the

dislocation density types corresponding to each stage of deformation are discussed and the recrystallization grade is calculated.

Keywords: synchrotron x-ray diffraction; aluminium alloys; hot deformation; continuous dynamic recrystallization; dynamic recovery.

1 Introduction

Many metals undergo dynamic recrystallization (DRX) during hot deformation and their stacking fault energies (SFE) determine the type of recrystallization. Discontinuous dynamic recrystallization (dDRX) is linked to materials with low and moderate SFE which undergo nucleation and grain growth [1,2]. Two mechanisms have been suggested for the changes of the microstructure of high SFE materials during large plastic deformations: 1) continuous dynamic recrystallization (cDRX), and 2) geometric dynamic recrystallization (gDRX). The cDRX requires a change in texture [1-3] and involves the progressive formation and rotation of subgrains. During this process, subgrains increase their wall dislocation density provoking a misorientation increment and low angle grain boundaries (LAGBs) transform into high angle grain boundaries (HAGBs) [3-9]. In gDRX texture remains unchanged [10-11] and it fulfils the Taylor theory basis [12], requiring subgrain formation and subsequent migration and pinching off of original HAGBs [8]. Both mechanisms can occur at the same time [13-14] and the third-generation of synchrotron radiation sources can be a powerful tool to track and identify these physical phenomena occurring during thermomechanical processes [15].

The main goals of this work are to extract microstructural information from a high temperature torsion test using in-situ high energy synchrotron radiation diffraction (HEXRD) and to clarify if the formed HAGB are mainly a consequence of the transformation from LAGB (cDRX) or by HAGB migration (gDRX) [16].

2 Materials and methods

The AA6082 aluminium alloy, produced by hot extrusion and aged to T6 condition, showed rod-like shape grains elongated in the extrusion direction with approximately 1000 μm in length and 15 μm in diameter. The specimen was in–situ tested by HEXRD in transmission mode during hot torsion at the P07 beamline of PETRA III at the Deutsches Elektronen-Synchrotron (DESY) in Hamburg [17]. A cylindrical sample was machined to 4 mm diameter and a gauge length of 20 mm with 2 mm transition radius to the 35 mm length and 10 mm diameter heads with its axis sample aligned in the extrusion direction. For torsion, a stepping motor driven machine with free-end movement was used at constant 0.01 s^{-1} (surface) strain rate. The test temperature was 400 °C (± 5°C) and it was measured and controlled by K-type thermocouples close to the sample surface. The incident beam, with E = 87.1 keV (λ = 0.01423 nm), was placed close to the non-rotating side and ~ 0.1 mm below the outer surface of the sample. Slit dimensions were set to 0.7 mm (horizontal) x 0.2 mm (vertical) and the sample-detector distance was 1457 mm (calibrated with a LaB_6 capillary). Diffracted images were collected every second in a 2-D Perkin-Elmer 1622 flat panel detector with an array of 2048x2048 pixels. A schematic zenithal view of the in-situ synchrotron measurement is shown in Fig. 1.

Effective strain and stress close to the surface were calculated as:

$$\varepsilon_{eff} = \frac{1}{\sqrt{3}} \frac{2\pi N}{1} \frac{R}{L} = \frac{1}{\sqrt{3}} \theta \frac{R}{L} \qquad \text{Eq. (1)}$$

$$\sigma_{eff} = \frac{\sqrt{3}M}{2\pi R^3} (3 + m + n) \qquad \text{Eq. (2)}$$

with N the number of revolutions, R the gauge radius (2 mm), L the gauge length (20 mm), M the torque, m the strain rate sensitivity (0.18), and n the strain hardening coefficient calculated as $(\partial\ ln\ M / \partial\ ln\ \theta)$ that varies during the experiment. A more detailed explanation of different parameters can be found in [18-19].

3 Results

Debye-Scherrer rings of the collected images were processed using ImageJ [20] to produce the azimuthal angle (ψ) - effective strain (AS) - plot [15]. Fig. 2 shows the AS-plot for the Al-220 crystallographic plane. Initial high intensity regions can be distinguished around $\psi \sim 35°$, ~ 90°, ~ 145°, 215°, 270°, and ~ 325° and less intense around $\psi \sim 45°$, 135°, 225°, and 315° indicating a strong (111)- and a less intense (200)-fibre textures. These high intensity regions broaden monotonically up to an effective strain of $\varepsilon_{eff} \sim 0.7$ where the initial texture breakdown occurs as a consequence of misorientation formation due to dynamic recovery [15]. Up to $\varepsilon_{eff} \sim 1.1$ little variations can be observed. Finally, the strain-lines develop new changes indicative of a new texture.

The collected 2D-images were integrated in sectors as a function of the azimuthal angle using the Input4MAUD software [21] and exported into MAUD software [22] for Rietveld analysis ($10\% \leq R_{wnb} \leq 20\%$). The dislocation densities were determined with the Williamson-Smallman relations [23]:

$$\rho_D = \frac{3p}{D_{eff}^2} \qquad \text{Eq. (3)}$$

$$\rho_S = \frac{ke_{RMS}^2}{Fb^2} \qquad \text{Eq. (4)}$$

where p is the number of dislocations on the coherently scattering domain from a diffraction point of view (hereafter crystallite for the sake of brevity) face of the block structure (=1), D_{eff} is the crystallite diameter, K depends on the lattice (=16.1), e_{RMS} is the root-mean square from Rietveld refinements, F is the energy interaction factor of dislocations (=1), and b is the Burger's vector.

Fig. 3 shows the evolution of a) σ_{eff}, b) crystallite size and Taylor factor M (calculated as in [24]), and c) ρ_D, and lattice parameter a. The lower limit of the dislocation density can be calculated as [23]:

$$\rho = (\rho_D \rho_S)^{1/2} = \sqrt{\frac{3pk}{F}} \frac{e_{RMS}}{bD_{eff}} \quad \text{Eq. (5)}$$

The crystallite size after heating at 400°C and before deformation is around 3500 Å, decreasing to ~ 1500 Å up to $\varepsilon_{eff} \sim 0.25$ (same order of magnitude that in [25]) due to the formation of cells and subgrains in the early stages, while the dislocation density ρ increases from ~ $4x10^{12}$ m^{-2} to ~ $4x10^{13}$ m^{-2} (Fig. 3 c). By increasing the strain, the crystallites increase their size up to around 4500 Å at $\varepsilon_{eff} \sim 1.1$ by wall sharpening, re–arrangement of dislocations, and a total decrement of ρ down to ~ $1x10^{12}$ m^{-2}. Simultaneously, M decreases continuously, evidencing texture variations. The crystallite size decreases to 3500 Å at $\varepsilon_{eff} \sim 1.5$ with negligible variation in ρ.

4 Discussion

The total dislocation density according to the Kocks-Mecking equation [26] reads as:

$$\rho_{K-M} = (\sigma_{eff}/\alpha M b \mu)^2 \quad \text{Eq. (6)}$$

where σ is the effective stress, $\alpha = 0.5$, M is taken from Fig. 3, and μ is the shear modulus equal to 21.6 GPa [27]). From Fig. 2 can also be inferred that a new (200) texture starts to develop from $\varepsilon_{eff} \sim 1.1$ with high intensity regions between ~ 40°-140° and between ~ 220°-320°. This texture is roughly similar to that formed during rolling at high temperature in a 6082 aluminium alloy [28] and it is used to validate, in first approach, the use of the Kocks-Mecking equation in this study. The calculated ρ_D and ρ define the upper and lower limits of the total dislocation density, respectively (Fig. 3c). During the early stages of deformation when both ρ_D and ρ increase (up to $\varepsilon_{eff} \sim 0.25$), $\rho_{K\text{-}M}$ is close to the average of the internal dislocation density ρ due to the cell and subgrain formations. When dynamic recovery occurs $\rho_{K\text{-}M}$ approaches to ρ_D,

which represents the wall dislocation density, becoming both roughly equal between ε_{eff} ~ 0.7-1.1. Above ε_{eff} ~ 1.1 $\rho_{K\text{-}M}$ slightly decreases when compared to ρ_D due to the wall dislocation absorption by the existent and new created boundaries. Consequently, the stress softening is produced mainly by the texture change up to ~ 0.7 of strain, and due to the annihilation of dislocations by cDRX above ~ 0.7 of strain.

The variation of the lattice parameter *a* is directly connected to the Swift or texture effect [29]: recovery *a* initially increases up to ε_{eff} ~ 0.25, then it decreases until the initial texture breaks down at ε_{eff} ~ 0.7, and finally it increases up to ε_{eff} ~ 2.7. The crystallite size and dislocation densities are constant from ε_{eff} ~1.5 while *a* monotonically increases, interpreted as grain rotation and accommodation of misorientations by changing the lattice parameter, ascribed to the cDRX.

Pole figures produced during Rietveld refinements were exported to the software MTEX [30] to obtain the misorientation angle distribution (Fig. 4a). Only the evolution of the HAGBs is analysed (the maximum resolution of MTEX is set to 5° which is assumed as the error). The fraction of HAGBs, considered as a trend, is calculated as the relative area variations at different ε_{eff} compared with the condition at ε_{eff} ~ 0.7:

$$\%\, HAGBs = \frac{[Area\ total - Area_{15-62.8}]_{\ \varepsilon eff} - [Area\ total - Area_{\ 15-62.8}]_{\ \varepsilon eff\ \sim 0.7}}{[Area\ total - Area_{\ 15-62.8}]_{\ \varepsilon eff\ \sim 0.7}} \times 100 \qquad \text{Eq. (7)}$$

During the early stages of deformation and up to ε_{eff} ~ 0.7 the HAGBs decrease from ~ 100% to 0% (Fig. 4b), in agreement with the formation of LAGBs by dynamic recovery. Subsequently dislocations arrange at LAGBs increasing their misorientation constantly and increasing the fraction of HAGBs [31] up to ~ 65% at ε_{eff} = 2.7. The fraction of HAGBs can be related directly with the % of recrystallization.

5 Conclusions

The following conclusions are drawn:

- In-situ synchrotron radiation is a powerful tool to quantify the evolution of texture and the size of coherently scattering domains in an Al-Si-Mg alloy undergoing continuous dynamic recrystallization.
- Up to ~ 0.25 of strain, subgrain formation occurs while the crystallite size is reduced. As deformation increases up to ~ 1.1 of strain, the internal dislocation density decreases while the crystallite increases by dynamic recovery remaining onwards constant.
- Grain rotation of crystallites was proved by studying the lattice parameter evolution.
- The ratio formation of high angle grain boundaries is calculated by analysing the misorientation angle distributions.
- The dislocation density types corresponding to each stage of deformation are characterised. Initially, the internal dislocation density prevails and wall dislocations become relevant when recovery takes place.

Acknowledgements

The financial support from the FWF (Austrian Science Fund) project P27471-N19 is greatly acknowledged. The authors would like to thank the allocation of beamline at the P07-HEMS beamline of PETRA III (DESY) in the framework of proposal I-20160441 EC, and to R.H. Buzolin for helping with the synchrotron experiments.

[1] F.J. Humphreys, M. Hatherly, Recrystallization and related annealing phenomena, 2nd ed. Elsevier, Oxford, 2004.
[2] T. Sakai, A. Belyakov, R. Kaibyshev, H. Miura, J.J. Jonas, Dynamic and post-dynamic recrystallization under hot, cold and severe plastic deformation conditions, Prog. Mater. Sci. 60 (2014) 130-207.
[3] S. Gourdet, F. Montheillet, An experimental study of the recrystallization mechanism during hot deformation of aluminium, Mater. Sci. Eng. A 283 (2000) 274-288.
[4] Q. Zang, H. Yu, Y-S. Lee, M-S. Kim, H-W. Kim, Hot deformation behavior and microstructure evolution of annealed Al-7.9Zn-2.7Mg-2.0Cu (wt%) alloy, J. Alloy Compd. 763 (2018) 25-33.

[5] O. Sitdikov, R. Garipova, E. Avtokratova, O. Mukhametdinova, M. Markushev, Effect of temperature of isothermal multidirectional forging on microstructure development in the Al-Mg alloy with nano-size aluminides of Sc and Zr, J. Alloy Compd. 746 (2018) 520-531.
[6] N. Su, R. Guan, X. Wang, Y. Wang, W. Jiang, H. Liu, Grain refinement in an Al-Er alloy during accumulative continuous extrusion forming, J. Alloy Compd. 680 (2016) 283-290.
[7] J. Zhao, J. Zhong, F. Yan, F. Chai, M. Dargusch, Deformation behaviour and mechanisms during hot compression at supertransus temperatures in Ti-10V-2Fe-3Al, J. Alloy Compd. 710 (2017) 616-627.
[8] Y.C. Lin, J. Huang, D.-G. He, X.-Y. Zhang, Q. Wu, L.-H. Wang, C. Chen, K.-C. Zhou, Phase transformation and dynamic recrystallization behaviors in a Ti55511 titanium alloy during hot compression, J. Alloy Compd. 795 (2019) 471-482.
[9] M. Suresh, A. Sharma, A.M. More, R. Kalsar, A. Bisht, N. Nayan, S. Suwas, Effect of equal channel angular pressing (ECAP) on the evolution of texture, microstructure and mechanical properties in the Al-Cu-Li alloy AA2195, J. Alloy Compd. 785 (2019) 972-983.
[10] H. J. McQueen, O. Knustand, N. Ryum, J.K., Solberg, Microstructural evolution in Al deformed to strains of 60 at 400°C, Scripta Metall. Mater. 19 (1985) 73-78.
[11] J.K. Solberg, H.J. McQueen, N. Ryum, E. Nes, Influence of ultra-high strains at elevated temperatures on the microstructure of aluminium. Part I, Philos. Mag. A 60 (1989) 447-471.
[12] H.J. McQueen, M.E. Kassner, Comments on 'a model of continuous dynamic recrystallization' proposed for aluminium', Scripta Mater. 51 (2004) 461-465.
[13] L.D. Pari Jr., W.Z. Misiolek, Theoretical predictions and experimental verification of surface grain structure evolution for AA6061 during hot rolling, Acta Mater. 56 (2008) 6174-6185.
[14] N.P. Gurao, A.O. Adesola, A.G. Odeshi, J.A. Szpunar, On the evolution of heterogeneous microstructure and microtexture in impacted aluminium-lithium alloy, J. Alloy Compd. 578 (2013) 183-187.
[15] K.-D. Liss, K. Yan, Thermomechanical processing in a synchrotron beam, Mater. Sci. Eng. A 528 (2010) 11-27.
[16] K. Huang, R.E. Logé, A review of dynamic recrystallization phenomena in metallic materials, Mater. Design. 111 (2016) 548-574.
[17] N. Schell, A. King, F. Beckmann, T. Fischer, M. Müller, A. Schreyer, The high energy materials science beamline (HEMS) at PETRA III, Mater. Sci. Forum 772 (2014) 57-61.
[18] D.S. Fields, W.A. Backofen, Determination oft he strain hardening characteristics by torsion testing, Proc. ASTM 57 (1957) 1259-1272.
[19] F. Montheillet, M. Cohen, J.J. Jonas, Axial stress and texture development during the torsion testing of Al, Cu and α-Fe, Acta Metall. 32 (1984) 2077-2089.
[20] <http://rsbweb.nih.gov/ij/>
[21] L. Raue, Input4MAUD: an efficient program for automatic two-dimensional diffraction image series input and/or batch refinement with MAUD, J. Appl. Crystallogr. 47 (2014) 2081-2085.
[22] L. Lutterotti, S. Matthies, H.-R. Wenk, A.S. Schultz, J.W. Richardson, Combined texture and structure analysis of deformed limestone from time-of-flight neutron diffraction spectra, J. Appl. Phys. 81 (1997) 594-600.
[23] G.K. Williamson, R.E. Smallman, III. Dislocation densities in some annealed and cold-worked metals from measurements on the X-ray Debye-Scherrer spectrum, Philos. Mag. 1 (1956) 34-46.
[24] D. Canelo-Yubero, G. Requena, F. Sket, C. Poletti, F. Warchomicka, J. Daniels, N. Schell, A. Stark, Load partition and microstructural evolution during in situ hot deformation of Ti-6Al-6V-2Sn alloys, Mater. Sci. Eng. A 657 (2016) 244-258.
[25] J. Gubicza, N.Q. Chinh, Z. Horita, T.G. Langdon, Effect of Mg addition on microstructure and mechanical properties of aluminium, Mater. Sci. Eng. A 387-389 (2004) 55-59.
[26] H. Mecking, U.F. Kocks, Kinetics of flow and strain-hardening, Acta Metall. 29 (1981) 1865-1875.
[27] E. Kabliman, P. Sherstnev, Integrated Modeling of Strength Evolution in Al-Mg-Si Alloys during Hot Deformation, Mater. Sci. Forum 765 (2013) 429–433.
[28] F. Pérocheau, J.H. Driver, Texture gradient simulations for extrusion and reversible rolling of FCC metals, Int. J. Plasticity 16 (2000) 73-89.
[29] H. W. Swift, Length changes in metals under torsional overstrain, Engineering 163 (1947) 253-257.
[30] F. Bachmann, R. Hielscher, H. Schaeben, Texture analysis with MTEX-Free and open source software toolbox, Solid State Phenom. 160 (2010) 63-68.
[31] M. C. Poletti et al 2019 J. Physics.: Conf. Ser. 1270 012049.

Captions

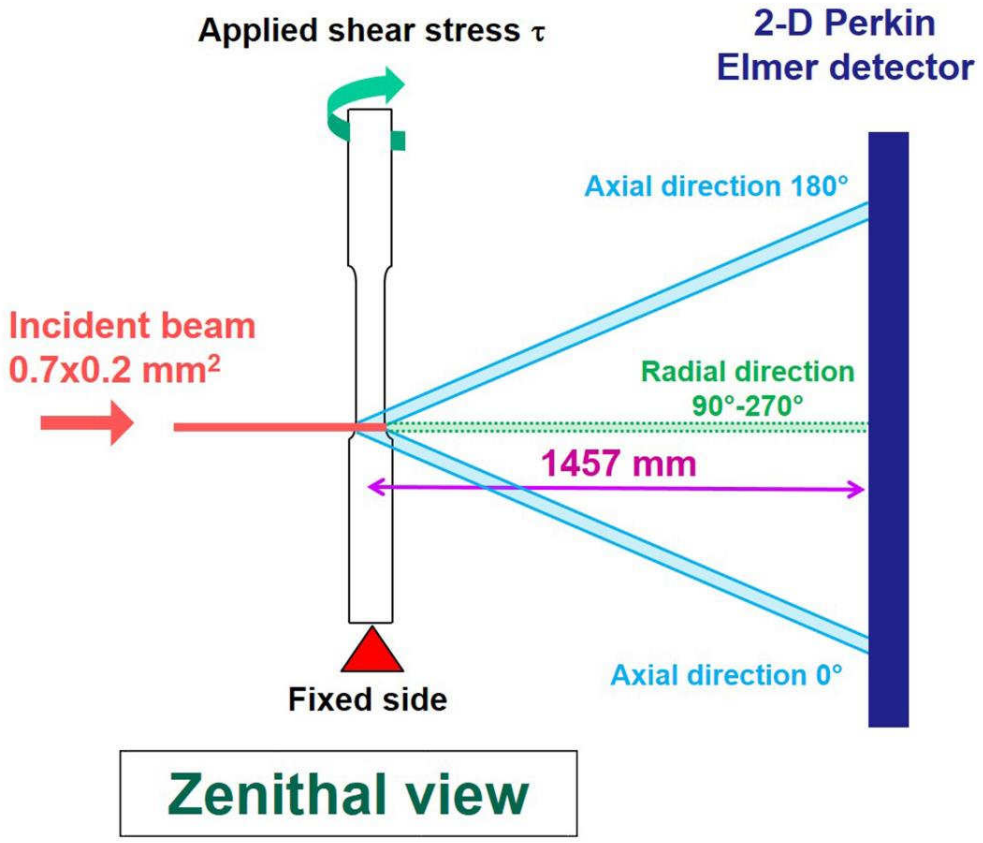

Fig. 1. Schematic zenithal view of the in-situ synchrotron diffraction experiment.

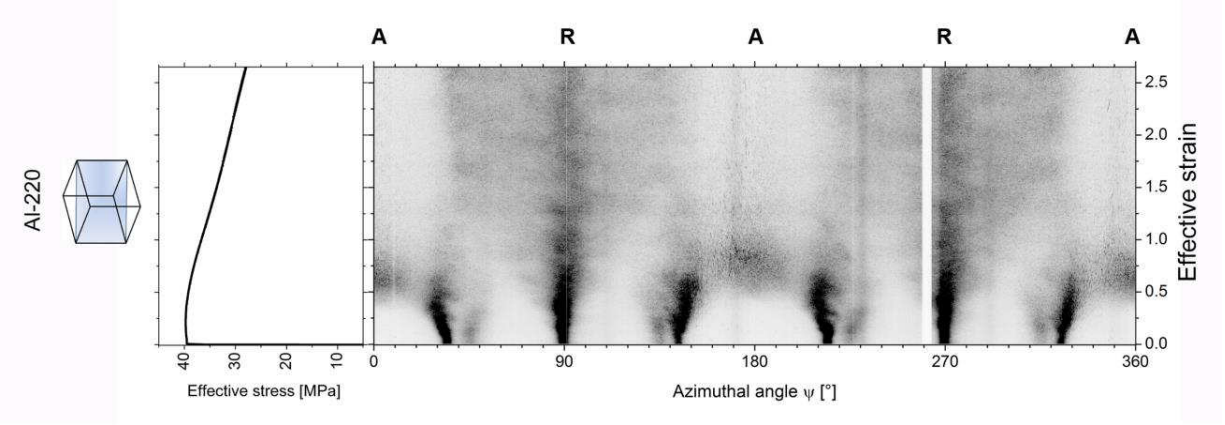

Fig. 2. AS-plot for the Al-220 reflection. The azimuthal angle is indicated at the bottom and axial (A) and radial (R) directions at the top.

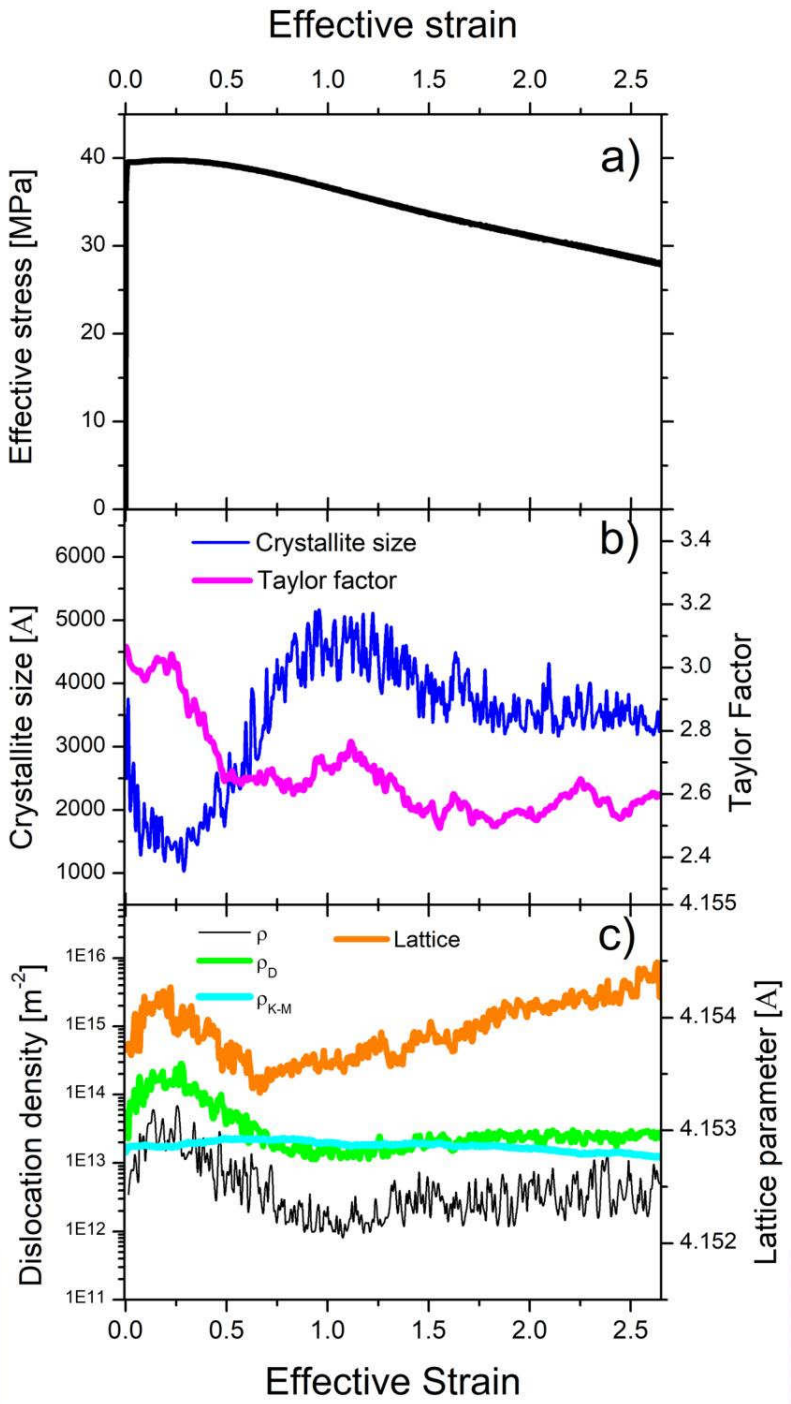

Fig. 3. Evolution of the different parameters as a function of the effective strain: a) effective stress, b) crystallite size and Taylor factor, and c) dislocation densities and lattice parameter.

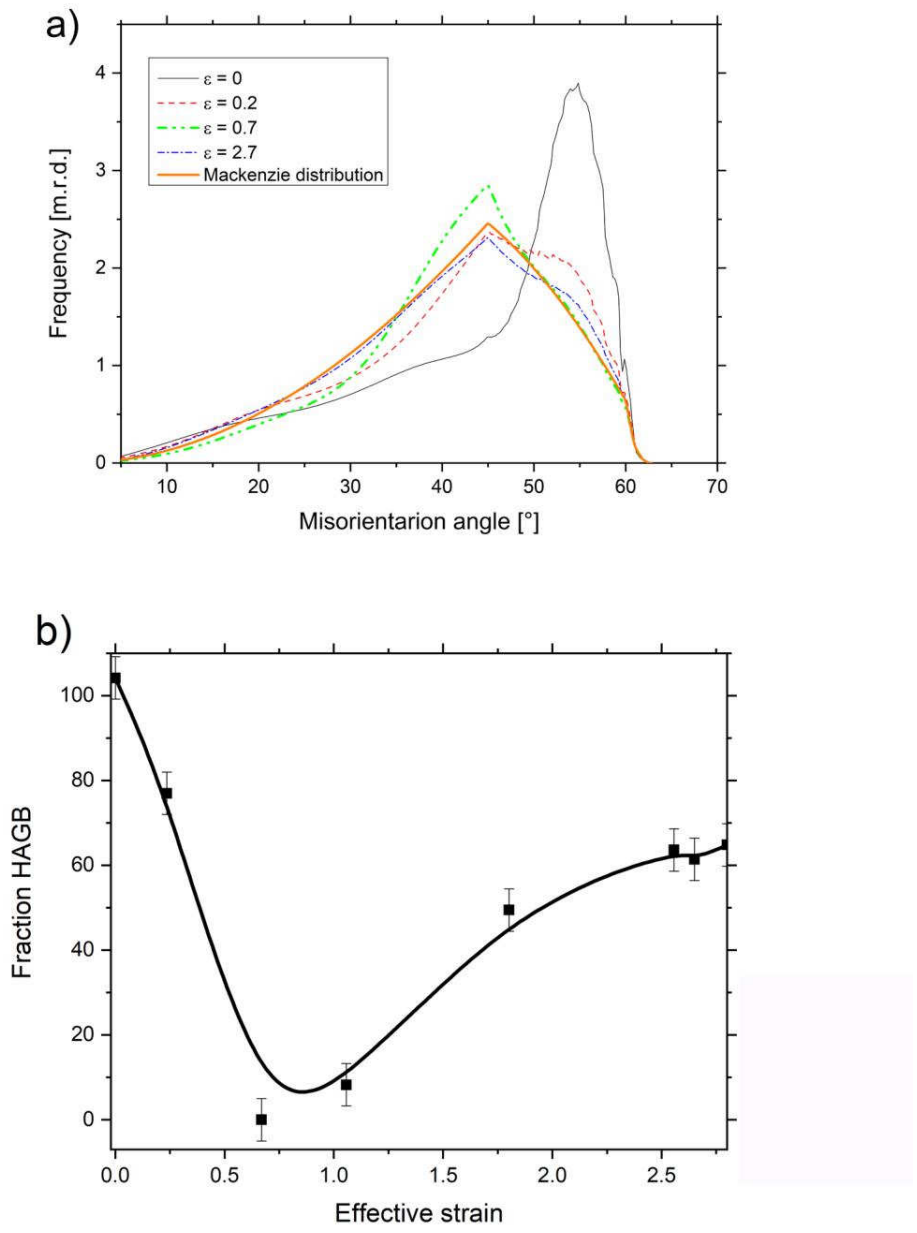

Fig. 4. a) Misorientation distribution at different effective strains and the Mackenzie distribution. b) Fraction of HAGBs.